

A BERNOULLI PHASE-FITTED FINITE DIFFERENCE METHOD AND WAVENUMBER-EXPLICIT ANALYSIS FOR THE ONE-DIMENSIONAL HELMHOLTZ EQUATION

ANSGAR JÜNGEL, PANCHI LI, ZHIWEI SUN, AND ZHIWEN ZHANG

ABSTRACT. We propose a Bernoulli phase-fitted (BPF) finite difference method for the Helmholtz equation on the interval $(0, L)$ with impedance boundary conditions. The scheme is derived from a complexified Scharfetter–Gummel discretization of the one-way factorization of the Helmholtz operator. It yields both a phase-fitted interior discretization and exact discrete impedance boundary closures. For the homogeneous problem, the method is exact for plane waves, so the scheme introduces neither numerical dispersion in the interior nor artificial reflection at the boundaries. For the inhomogeneous problem, we prove well-posedness, derive wavenumber-explicit stability estimates, and establish second-order consistency and convergence valid for all $kh \notin \pi\mathbb{Z}$, where k is the wavenumber and h the grid size. In particular, under the fixed-resolution condition $kh \leq s_0$ for some $0 < s_0 < \pi$ together with $kL \geq \pi$, the constants in the error bounds remain uniform with respect to the wavenumber, yielding a pollution-free convergence theory in the principal Nyquist regime. Numerical experiments confirm the theoretical analysis and show favorable performance compared with standard and dispersion-corrected finite difference methods.

1. INTRODUCTION

The Helmholtz equation is a fundamental model for time-harmonic wave propagation in acoustics, electromagnetics, and seismic imaging. In the high-frequency regime, characterized by large wavenumbers k , its solutions are highly oscillatory, and their accurate numerical approximation remains a central challenge in scientific computing. A well-known difficulty is the pollution effect [1, 2, 12, 21, 22]: For standard discretization methods, as

Date: May 21, 2026.

2020 Mathematics Subject Classification. 35J05, 65N06, 65N12, 65N15.

Key words and phrases. Bernoulli Phase-Fitted method, Helmholtz problem, impedance boundary conditions, Scharfetter–Gummel discretization, wavenumber-explicit analysis, pollution-free convergence.

The first author acknowledges partial support from the Austrian Science Fund (FWF), grant 10.55776/PAT2687825, and from the Austrian Federal Ministry for Women, Science and Research and implemented by ÖAD, project MultHeFlo. This work has received funding from the European Research Council (ERC) under the European Union’s Horizon 2020 research and innovation programme, ERC Advanced Grant NEUROMORPH, no. 101018153. The research of Z. Zhang was supported by the National Natural Science Foundation of China (Project 92470103), the Hong Kong RGC grant (Projects 17304324 and 17300325), the Seed Funding Programme for Basic Research (HKU), and the Hong Kong RGC Research Fellow Scheme 2025. For open-access purposes, the authors have applied a CC BY public copyright license to any author-accepted manuscript version arising from this submission.

the wavenumber k increases, the numerical error cannot in general be controlled solely by maintaining a fixed number of degrees of freedom per wavelength. Consequently, to achieve a prescribed accuracy, the total number of degrees of freedom must grow faster than the natural scaling $O(k^d)$, where d is the spatial dimension.

A large body of work has therefore been devoted to mitigating the pollution effect in Helmholtz discretizations. In the context of finite element methods, high-order and hp -FEM techniques can substantially reduce pollution when the polynomial degree is increased together with mesh refinement [23, 24, 26]. Related approaches include discontinuous Galerkin formulations, boundary element methods, and multiscale methods, all of which have been developed to improve robustness in the high-frequency regime [14, 15, 17, 25, 27]. Another important class consists of Trefftz and wave-based methods, in which the approximation spaces are built from local solutions of the underlying differential equation and hence the incorporate oscillatory behavior directly [4, 18, 19, 20]. These developments show that controlling the phase accuracy of the discretization is central to the design of robust high-frequency methods.

Within the finite difference framework, a common approach is to design stencils with adjustable coefficients aimed at minimizing dispersion errors. This viewpoint has led to a variety of optimized compact schemes [5, 6] and dispersion-minimizing schemes [10, 11, 28, 32] in multiple space dimensions. Another important line of work is based on the use of a *shifted wavenumber*, chosen to ensure that the discrete phase velocity better matches the exact velocity; see, e.g., [8, 9]. More recently, asymptotic dispersion correction was developed for general finite difference schemes, providing a systematic way to improve the accuracy of discrete Helmholtz operators [7].

For the one-dimensional Helmholtz equation, even stronger results are possible. Exact three-point finite difference schemes were constructed for homogeneous problems [31], and pollution-free finite difference schemes were also proposed for nonhomogeneous equations [30]. The corresponding analyses are based on Taylor expansion and are therefore established in a small- kh regime only, where h is the grid size. Recent Fourier-based analyses [16] show that one can derive sharp wavenumber-explicit error estimates; however, the rigorous results focus on the classical centered three-point scheme with Dirichlet boundary conditions. Hence, rigorous pollution-free convergence results remaining valid throughout the full Nyquist band $0 < kh < \pi$ are still largely unavailable, particularly in the presence of impedance boundary conditions.

1.1. Motivation and general framework. The starting point is the observation that the one-dimensional Helmholtz operator admits the factorization

$$(1) \quad \partial_{xx} + k^2 = (\partial_x + ik)(\partial_x - ik),$$

which separates the left- and right-traveling components of the wave. The corresponding one-way operators annihilate the elementary plane waves $e^{\pm ikx}$, suggesting that one may discretize these first-order factors directly rather than approximate the second-order operator only through a standard three-point stencil.

Motivated by this factorization, we develop a finite difference scheme based on a complexified version of the classical Scharfetter–Gummel (SG) discretization [3, 29]. The SG scheme is widely recognized for its ability to include the local first-order flux directly within the discrete operator. By replacing the real drift parameter with the purely imaginary quantity ik , we obtain discrete one-way operators that naturally approximate the Helmholtz factors $\partial_x \pm ik$. Their composition yields a new Bernoulli phase-fitted (BPF) finite difference discretization for the Helmholtz equation.

Within the interior domain, the resulting three-point formula is closely related to phase-fitted and shifted-wavenumber discretizations for the one-dimensional Helmholtz equation [7, 13, 30]. In particular, for homogeneous interior equations it recovers the three-point scheme [31] associated with the shifted wavenumber, while in the presence of a source term, it introduces a scaled right-hand side through the Bernoulli factor $|B(ikh)|^2$; see Remark 1. The present factorization-based construction is particularly natural in the impedance setting: The SG discretization preserves the local exactness of the one-way plane waves, while the factorized form carries this property to the boundary. As a result, the scheme yields exact discrete impedance boundary closures and, at the same time, provides a unified, structure-preserving framework for the well-posedness and convergence analysis.

From an analytical point of view, the main question is whether the BPF construction admits rigorous wavenumber-explicit and pollution-free error estimates on the full Nyquist band $0 < kh < \pi$. Existing dispersion-corrected finite difference analyses for the one-dimensional Helmholtz equation typically yield error bounds of order $O(k^2h^2)$ [7]. In the Dirichlet setting, the analysis in [30] suggests that an $O(h^2)$ regime may be attainable. A difficulty is that classical Taylor expansion alone does not provide estimates uniformly in the wavenumber, since derivatives of oscillatory solutions typically scale with k . Our approach is inspired by recent Fourier-based analyses for Dirichlet problems [16]. In the present setting, however, the impedance boundary closures introduce an additional difficulty. To overcome this obstacle, we exploit the plane-wave exactness of the scheme to lift the Helmholtz kernel component, and thereby isolate a zero-trace remainder. The subsequent analysis can then be carried out by combining a sine expansion with a Fourier-symbol analysis. In this way, the factorization-based structure of the scheme leads to the wavenumber-explicit stability bounds and uniform convergence estimates established below.

1.2. Main results and contributions. In this paper, we consider the one-dimensional Helmholtz problem with impedance boundary conditions

$$u''(x) + k^2u(x) = f(x), \quad x \in (0, L), \quad u'(0) - ik u(0) = g_0, \quad u'(L) + ik u(L) = g_L,$$

where $g_0, g_L \in \mathbb{C}$ prescribe the incoming wave data at the two boundaries.

For this problem, we establish a wavenumber-explicit analysis of the proposed BPF finite difference scheme. For the homogeneous equation, namely $f(x) = 0$, we show that the scheme reproduces the sampled plane-wave solutions exactly, both in the interior and at the discrete boundary closures. For the inhomogeneous problem, we prove stability,

consistency, and second-order convergence estimates for all $kh \notin \pi\mathbb{Z}$. A representative form of the convergence estimate for the grid error e is

$$k\|e\|_{0,h} + |e|_{1,h} \lesssim h^2,$$

with constants given explicitly in terms of kh and kL . In particular, under the conditions $kh \leq s_0 < \pi$ for some $s_0 > 0$ and $kL \geq \pi$, these constants remain uniformly bounded with respect to the wavenumber. The condition $kh \leq s_0 < \pi$ corresponds to a number of more than two grid points per wavelength (PPW), since $\text{PPW} = 2\pi/(kh) \geq 2\pi/s_0 > 2$, while $kL \geq \pi$ means that the interval $(0, L)$ contains at least half a wavelength. Thus, in the principal Nyquist regime, the method admits a natural pollution-free interpretation under the fixed resolution $kh \leq s_0 < \pi$. Equivalently, in such a regime, the second-order estimate $O(h^2)$ may also be interpreted as an $O(k^{-2})$ decay with respect to the wavenumber. Our theoretical findings are further confirmed by numerical experiments. The main contributions are:

- We propose a BPF finite difference scheme for the one-dimensional Helmholtz equation with impedance boundary conditions, derived from a complexified Scharfetter–Gummel discretization; see Sections 2.2–2.3.
- We prove that the scheme is exact for the homogeneous problem: It reproduces plane waves exactly, with no numerical dispersion in the interior and no artificial reflection at the boundaries (Proposition 2).
- We develop a wavenumber-explicit analysis based on a Fourier-symbol viewpoint, exact plane-wave lifting, and the discrete factorization structure of the scheme. This yields stability, consistency, and second-order convergence estimates for all $kh \notin \pi\mathbb{Z}$ (Theorems 3, 12, and 13).
- In particular, we show that, under the fixed-resolution condition $kh \leq s_0 < \pi$ together with $kL \geq \pi$, the constants in the error estimates remain uniform with respect to the wavenumber, thereby establishing a pollution-free convergence theory in the principal Nyquist regime. Numerical experiments confirm the theory and demonstrate a favorable performance compared with standard and dispersion-corrected finite difference schemes.

1.3. Organization of the paper. The remainder of the paper is organized as follows. In Section 2, we derive the BPF discretization and prove its plane-wave exactness. Section 3 is devoted to the well-posedness and stability analysis of the discrete scheme. In Section 4, we establish consistency and convergence estimates. Finally, numerical experiments are presented in Section 5.

2. BERNOULLI PHASE-FITTED DISCRETIZATION

In this section, we derive the BPF finite difference discretization for the Helmholtz equation. As already mentioned, the construction is based on a factorization of the Helmholtz operator into one-way components and a complexified version of the classical Scharfetter–Gummel discretization.

2.1. Helmholtz factorization and grid notation. Recall the one-dimensional Helmholtz equation

$$(2) \quad u_{xx}(x) + k^2 u(x) = f(x), \quad x \in (0, L),$$

with the impedance (radiation) boundary conditions

$$(3) \quad u_x(0) - ik u(0) = g_0, \quad u_x(L) + ik u(L) = g_L,$$

where $g_0, g_L \in \mathbb{C}$. The decomposition $\partial_{xx} + k^2 = (\partial_x + ik)(\partial_x - ik)$ separates the Helmholtz operator into two first-order one-way operators associated with opposite propagation directions. In particular, $(\partial_x + ik)e^{-ikx} = 0$ and $(\partial_x - ik)e^{ikx} = 0$ for $x \in [0, L]$, so that the operators annihilate outgoing and incoming plane waves, respectively. This structure motivates the construction of discrete operators that preserve these one-way propagation properties.

To formulate the discretization, we introduce the computational grid. The interval $[0, L]$ is divided into n uniform subintervals of length $h := L/n$ with grid points $x_i := ih$ for $i = 0, 1, \dots, n$. For grid functions $v = \{v_i\}_{i=0}^n$ and $w = \{w_i\}_{i=0}^n$, we define the discrete inner product and L^2 norm on the interior grid by

$$(v, w)_h := h \sum_{i=1}^{n-1} v_i \bar{w}_i, \quad \|v\|_{0,h}^2 := (v, v)_h,$$

where \bar{w}_i denotes complex conjugation. The forward difference operator and the associated discrete H^1 seminorm are defined as

$$(\nabla_h v)_i := \frac{v_{i+1} - v_i}{h}, \quad i = 0, \dots, n-1, \quad |v|_{1,h}^2 := h \sum_{i=0}^{n-1} |(\nabla_h v)_i|^2.$$

Finally, the standard three-point approximation to the second derivative equals

$$(\Delta_h v)_i := \frac{v_{i+1} - 2v_i + v_{i-1}}{h^2}, \quad i = 1, \dots, n-1.$$

2.2. Complexified Scharfetter–Gummel operators. To discretize the one-way operators appearing in the Helmholtz factorization (1), we draw inspiration from the Scharfetter–Gummel (SG) discretization [3, 29], which was originally developed for semiconductor drift–diffusion models. The one-dimensional drift–diffusion equation can be written in the flux form as

$$\partial_t u = \partial_x F, \quad F = \partial_x u - vu = (\partial_x - v)u,$$

where v denotes the drift velocity. The SG scheme approximates the flux at cell interfaces by locally solving the stationary flux equation, which leads to

$$(4) \quad F_{i+1/2} = \frac{1}{h} (B(hv)u_{i+1} - B(-hv)u_i).$$

Here, $B(z)$ for $z \in \mathbb{C}$ denotes the Bernoulli function

$$B(z) = \frac{z}{e^z - 1} \quad \text{for } z \neq 0, \quad \text{and} \quad B(0) = 1.$$

The following useful properties are used later:

$$(5) \quad B(-z) = e^z B(z), \quad B(-z) - B(z) = z.$$

To adapt this idea to the Helmholtz equation, we complexify the SG flux by replacing the real drift velocity v in (4) with the imaginary wavenumber ik . This leads to the discrete one-way operators

$$\begin{aligned} (D_k^+ u)_i &:= \frac{1}{h} \left(B(ikh) u_{i+1} - B(-ikh) u_i \right), \\ (D_k^- u)_i &:= \frac{1}{h} \left(B(-ikh) u_i - B(ikh) u_{i-1} \right). \end{aligned}$$

These operators preserve the plane-wave structure of the Helmholtz equation. Indeed (see Proposition 2), we have

$$D_k^+ e^{ikx_i} = 0, \quad D_k^- e^{-ikx_i} = 0,$$

so that the discrete operators annihilate the corresponding one-way plane waves exactly.

2.3. BPF finite difference scheme. We now construct the discrete Helmholtz operator by composing the one-way operators D_k^+ and D_k^- introduced above. Applying these operators to the Helmholtz equation (2) together with the boundary conditions (3) leads to the discrete system

$$(6) \quad \begin{cases} D_k^- D_k^+ u_i = f_i, & i = 1, \dots, n-1, \\ D_k^+ u_0 = m(kh) g_0, & D_k^- u_n = m(kh) g_L, \end{cases}$$

where $f_i := f(x_i)$. The complex-valued correction factor

$$(7) \quad m(s) = e^{-is/2} \cos(s/2)$$

is chosen in such a way that the discrete boundary operators reproduce the exact plane-wave solutions; see Proposition 2. Note that $m(s) \neq 0$ for $s \in (0, \pi)$.

We further introduce the phase-fitted weight

$$\Theta(s) := |B(is)|^2 = B(is)B(-is), \quad s \in \mathbb{R},$$

which has the properties

$$\Theta(s) = \frac{s^2}{4 \sin^2(s/2)}, \quad s \notin 2\pi\mathbb{Z}, \quad \text{and} \quad 1 \leq \Theta(s) \leq \frac{\pi^2}{4}, \quad 0 \leq s \leq \pi.$$

A direct algebraic calculation (see Proposition 22 in Appendix A) shows that the composition $D_k^- D_k^+$ in (6) can be written in the three-point form

$$(8) \quad -\Theta(kh) (\Delta_h u)_i - k^2 u_i = f_i.$$

This representation shows that the BPF discretization is equivalent to a three-point finite difference scheme with a shifted wavenumber $\widehat{k} = k/\sqrt{\Theta(kh)}$. Hence, the method can be interpreted as a phase-fitted scheme: It inherits the pollution-free dispersion properties of shifted-wavenumber discretizations, while being derived systematically from the complexified SG flux.

Remark 1. In the homogeneous case $f_i = 0$, the interior scheme (8) coincides with the pollution-free finite difference method proposed in [13, 31], which eliminates the phase error by using the shifted wavenumber \widehat{k} . When a source term is present ($f_i \neq 0$), an alternative dispersion-corrected scheme was proposed in [7]:

$$-(\Delta_h u)_i - \widehat{k}^2 u_i = f_i.$$

In contrast, the BPF formulation introduces the scaled source term $f_i/\Theta(kh)$ in (8). Expanding $1/\Theta(kh)$ in powers of kh shows that, up to this expansion, the resulting method coincides with the second-order scheme proposed in [30]. This treatment of the source term is analogous to the approach used by [1] in the finite element framework; see also [16, Section 4] for a related discussion.

2.4. Exactness for plane waves. The BPF discretization reproduces the exact plane-wave solutions of the homogeneous Helmholtz equation. Indeed, consider the homogeneous problem ($f \equiv 0$). Its general solution on $(0, L)$ is

$$(9) \quad u(x) = \alpha e^{ikx} + \beta e^{-ikx}, \quad \alpha, \beta \in \mathbb{C}.$$

The coefficients α and β are determined by the impedance boundary conditions (3):

$$(10) \quad -2ik\beta = g_0, \quad 2ik e^{ikL}\alpha = g_L.$$

Proposition 2 (Exactness for plane waves). *Let $f \equiv 0$ and consider the continuous solution (9). Define the sampled sequence $u_i := u(x_i)$. Then it solves*

$$D_k^- D_k^+ u_i = 0, \quad (D_k^+ u)_0 = m(kh)g_0, \quad (D_k^- u)_n = m(kh)g_L,$$

where $i = 1, \dots, n-1$, recalling definition (7) of $m(s)$.

Proof. We first verify that the discrete one-way operators annihilate the corresponding plane waves. It holds for the outgoing wave e^{ikx} that

$$(D_k^+ e^{ikx})_i = \frac{e^{ikx_i}}{h} (B(ikh)e^{ikh} - B(-ikh)).$$

Using the identity $B(-z) = e^z B(z)$ with $z = ikh$ gives $(D_k^+ e^{ikx})_i = 0$. Similarly, we find that $(D_k^- e^{-ikx})_i = 0$. For the general solution (9), linearity yields

$$(D_k^- D_k^+ u)_i = \alpha D_k^- D_k^+ e^{ikx} + \beta D_k^- D_k^+ e^{-ikx} = 0,$$

which proves the interior equation. We infer from (61) and (62) that

$$(D_k^+ e^{-ikx})_0 = \frac{B(ikh)}{h} (e^{-ikh} - e^{ikh}) = -\frac{2i}{h} B(ikh) \sin(kh) = -2ik m(kh),$$

and similarly $(D_k^- e^{ikx})_n = 2ik m(kh)e^{ikL}$. We substitute (10) to obtain $(D_k^+ u)_0 = m(kh)g_0$ and $(D_k^- u)_n = m(kh)g_L$, finishing the proof. \square

As a consequence, the BPF discretization introduces neither numerical dispersion in the interior nor spurious reflection at the boundaries; the discrete solution coincides exactly with the continuous plane waves satisfying the impedance conditions.

3. STABILITY AND WELL-POSEDNESS

We establish the main stability result for the BPF scheme and prove the well-posedness of the discrete problem. Throughout this section, we assume that $kh \notin \pi\mathbb{Z}$, so that the Nyquist degeneracy is avoided and For brevity, we write $\Theta := \Theta(kh) = |B(ikh)|^2$.

Our goal is to derive estimates that are explicit with respect to the wavenumber and remain uniformly bounded under a fixed resolution constraint.

Theorem 3 (Well-posedness and k -explicit stability). *Let $u_h = \{u_i\}_{i=0}^n$ denote the solution to the BPF scheme (6). For $s := kh$ and $t := kL$, define*

$$(11) \quad A_0(s, t) := \frac{L}{\sqrt{2\Theta(s)}} \sec\left(\frac{s}{2}\right) + \frac{L}{2t} \sec^2\left(\frac{s}{2}\right),$$

Then, for any $kh \notin \pi\mathbb{Z}$, and for any source f and boundary data $g_0, g_L \in \mathbb{C}$, the BPF scheme admits a unique discrete solution satisfying

$$(12) \quad k\|u_h\|_{0,h} \leq A_0(kh, kL) \|f\|_{0,h} + \frac{\sqrt{L}}{2} (|g_0| + |g_L|),$$

$$(13) \quad \sqrt{\Theta} |u_h|_{1,h} \leq A_0(kh, kL) \|f\|_{0,h} + \frac{\sqrt{L}}{2} (|g_0| + |g_L|).$$

In particular, for any fixed $s_0 < \pi$, the quantities $A_0(kh, kL)$ remains uniformly bounded with respect to k whenever $kh \leq s_0$ and $kL \geq \pi$.

The proof of Theorem 3 is based on two key ingredients. First, we derive stability estimates for the discrete problem with homogeneous discrete radiation conditions. Second, we exploit the exactness result of Proposition 2, which shows that the BPF scheme reproduces the homogeneous plane-wave component exactly. This allows us to treat general boundary data by an exact lifting argument.

3.1. Reduction to homogeneous discrete radiation conditions. We first consider the BPF discretization with homogeneous discrete radiation conditions,

$$(14) \quad \begin{cases} D_k^- D_k^+ u_i = f_i, & i = 1, \dots, n-1, \\ (D_k^+ u)_0 = 0, & (D_k^- u)_n = 0. \end{cases}$$

This reduced problem contains the essential stability mechanism of the scheme. We isolate (14) since the contribution of the boundary data can be represented exactly by plane waves. Indeed, Proposition 2 shows that the homogeneous Helmholtz equation with impedance boundary data is reproduced exactly by the discrete BPF scheme at the nodal level. Consequently, the full discrete problem with general boundary data can be reduced to (14) by subtracting an exact plane-wave lifting.

We therefore first establish k -explicit stability estimates for (14). The lifting argument and the proof of the full stability theorem will be given in Section 3.4.

3.2. Basic flux and energy identities. We derive the basic estimates for the homogeneous-boundary problem (14). Since the one-way fluxes $D_k^+ u$ and $D_k^- u$ are naturally defined on staggered index sets, we slightly abuse the notation and write

$$\|D_k^+ u\|_{0,h}^2 := h \sum_{i=0}^{n-1} |D_k^+ u_i|^2, \quad \|D_k^- u\|_{0,h}^2 := h \sum_{i=1}^n |D_k^- u_i|^2.$$

We start with L^2 bounds for the discrete one-way fluxes associated with the homogeneous discrete radiation problem.

Lemma 4 (Flux estimate). *Let $u = \{u_i\}_{i=0}^n$ solve (14). Then*

$$(15) \quad \|D_k^+ u\|_{0,h}^2 + \|D_k^- u\|_{0,h}^2 \leq \frac{L^2}{\Theta} \|f\|_{0,h}^2.$$

Proof. Set $w_i := (D_k^+ u)_i$ for $i = 0, \dots, n-1$. We deduce from $D_k^- D_k^+ u = f$ and the definition of D_k^- that

$$B(-ikh) w_i - B(ikh) w_{i-1} = h f_i, \quad i = 1, \dots, n-1.$$

Using the identity $B(ikh) = e^{-ikh} B(-ikh)$ yields the recurrence

$$w_i = e^{-ikh} w_{i-1} + \frac{h}{B(-ikh)} f_i, \quad i = 1, \dots, n-1.$$

Since $(D_k^+ u)_0 = 0$, an iteration gives

$$w_i = \frac{h}{B(-ikh)} \sum_{j=1}^i e^{-ikh(i-j)} f_j, \quad i = 1, \dots, n-1.$$

Taking absolute values and using $|e^{-ikh(i-j)}| = 1$ and $|B(-is)|^2 = \Theta(s)$, we find that

$$|w_i| \leq \frac{h}{\sqrt{\Theta}} \sum_{j=1}^i |f_j| \leq \frac{h}{\sqrt{\Theta}} \sqrt{i} \left(\sum_{j=1}^i |f_j|^2 \right)^{1/2} \leq \frac{\sqrt{ih}}{\sqrt{\Theta}} \|f\|_{0,h}.$$

It follows from $\sum_{i=0}^{n-1} i \leq n^2/2$ and $nh = L$ that

$$(16) \quad \|D_k^+ u\|_{0,h} = \|w\|_{0,h} \leq \frac{L}{\sqrt{2\Theta}} \|f\|_{0,h}.$$

A completely analogous backward recursion, starting from $(D_k^- u)_n = 0$ leads to

$$(17) \quad \|D_k^- u\|_{0,h} \leq \frac{L}{\sqrt{\Theta}} \|f\|_{0,h}.$$

Combining (16) and (17) gives (15). \square

The next result relates the discrete one-way fluxes to the standard discrete H^1 norm and the boundary data.

Lemma 5 (Flux–energy relation). *For any $u = \{u_i\}_{i=0}^n$ and all $kh \notin \pi\mathbb{Z}$,*

$$(18) \quad \|D_k^+ u\|_{0,h}^2 + \|D_k^- u\|_{0,h}^2 = 2\Theta \cos(kh) |u|_{1,h}^2 + 2k^2 \|u\|_{0,h}^2 + k^2 h (|u_n|^2 + |u_0|^2).$$

Proof. Using the identity $B(-z) - B(z) = z$, we rewrite

$$(19) \quad (D_k^+ u)_i = \frac{B(ikh) u_{i+1} - B(-ikh) u_i}{h} = B(ikh) \nabla_h u_i - ik u_i,$$

$$(20) \quad (D_k^- u)_{i+1} = \frac{B(-ikh) u_{i+1} - B(ikh) u_i}{h} = B(ikh) \nabla_h u_i + ik u_{i+1}.$$

Hence, it follows that

$$|D_k^+ u_i|^2 + |D_k^- u_{i+1}|^2 = 2|B(ikh)|^2 |\nabla_h u_i|^2 + k^2 (|u_{i+1}|^2 + |u_i|^2) + T_{\text{cross}},$$

where the cross terms are collected into

$$T_{\text{cross}} = 2\Re\left(B(ikh) \nabla_h u_i \cdot \overline{ikh(\nabla_h u_i)}\right) = ikh\left(B(-ikh) - B(ikh)\right) |\nabla_h u_i|^2$$

Using $B(-z) - B(z) = z$ again, this gives

$$|D_k^+ u_i|^2 + |D_k^- u_{i+1}|^2 = (2|B(ikh)|^2 - k^2 h^2) |\nabla_h u_i|^2 + k^2 (|u_{i+1}|^2 + |u_i|^2).$$

Since $|B(is)|^2 = \Theta(s)$ and

$$2\Theta(s) - s^2 = \frac{s^2}{2 \sin^2(s/2)} - s^2 = \frac{s^2 \cos s}{2 \sin^2(s/2)} = 2\Theta(s) \cos s,$$

we obtain

$$|D_k^+ u_i|^2 + |D_k^- u_{i+1}|^2 = 2\Theta(kh) \cos(kh) |\nabla_h u_i|^2 + k^2 (|u_{i+1}|^2 + |u_i|^2).$$

Summing over $i = 0, \dots, n-1$ and multiplying by h yields (18). \square

As a byproduct of Lemmas 4 and 5, we have the following estimate.

Corollary 6 (Auxiliary energy bound). *Let u solve (14). For all $kh \notin \pi\mathbb{Z}$,*

$$(21) \quad \Theta \cos(kh) |u|_{1,h}^2 + k^2 \|u\|_{0,h}^2 + \frac{k^2 h}{2} (|u_0|^2 + |u_n|^2) \leq \frac{L^2}{2\Theta} \|f\|_{0,h}^2.$$

Remark 7 (Coercivity in the low-frequency regime). *Although (21) is valid for all $kh \notin \pi\mathbb{Z}$, it is coercive in the principal Nyquist regime $0 < kh < \pi$ only for $0 < kh < \pi/2$, since $\cos(kh)$ changes sign at $kh = \pi/2$. Hence, the estimate (21) alone is not sufficient to establish H^1 -control over the entire interval $0 < kh < \pi$, and an additional discrete energy identity, proved in the next subsection, is needed.*

3.3. Uniform stability for homogeneous discrete radiation conditions. We now establish k -explicit stability estimates for the homogeneous discrete radiation problem (14) that remain valid for all $kh \notin \pi\mathbb{Z}$, in particular for the whole principal Nyquist regime $0 < kh < \pi$. The key point is the discrete energy identity associated with the three-point formulation of the BPF scheme.

Lemma 8 (Discrete energy identity). *Let $u = \{u_i\}_{i=0}^n$ solve (14). Then*

$$(22) \quad \Theta |u|_{1,h}^2 - \frac{k^2 h}{2} (|u_0|^2 + |u_n|^2) - k^2 \|u\|_{0,h}^2 = \Re(f, u)_h.$$

Proof. According to the representation (8), we write the interior equation as

$$\Theta(kh) (\Delta_h u)_i + k^2 u_i = f_i, \quad i = 1, \dots, n-1.$$

Multiplying by $h \bar{u}_i$, summing over $i = 1, \dots, n-1$, and using the standard summation-by-parts identity

$$h \sum_{i=1}^{n-1} (\Delta_h u)_i \bar{u}_i = -|u|_{1,h}^2 + (\nabla_h u_{n-1} \bar{u}_n - \nabla_h u_0 \bar{u}_0),$$

we obtain

$$(23) \quad \Theta(kh) (|u|_{1,h}^2 - (\nabla_h u_{n-1} \bar{u}_n - \nabla_h u_0 \bar{u}_0)) - k^2 \|u\|_{0,h}^2 = (f, u)_h.$$

We next use the homogeneous discrete radiation conditions $D_k^+ u_0 = D_k^- u_n = 0$. Then we deduce from (19)-(20) that $B(ikh) \nabla_h u_0 = ik u_0$ and $B(ikh) \nabla_h u_{n-1} = -ik u_n$. Substitution into (23) yields

$$(24) \quad \Theta(kh) \left(|u|_{1,h}^2 + \frac{ik}{B(ikh)} (|u_n|^2 + |u_0|^2) \right) - k^2 \|u\|_{0,h}^2 = (f, u)_h.$$

Finally, since $B(z) = z/(e^z - 1)$, we have

$$\Re \left(\Theta(s) \frac{is}{B(is)} \right) = \Re(\Theta(s)(e^{is} - 1)) = \Theta(s)(\cos(s) - 1) = -\frac{s^2}{2}.$$

Using this formula and taking the real part of (24) gives (22). \square

We combine Corollary 6 and Lemma 8 to obtain global k -explicit L^2 and discrete H^1 bounds for the homogeneous-boundary problem.

Theorem 9 (Uniform stability for homogeneous radiation conditions). *The BPF scheme (14) with homogeneous radiation conditions admits a unique solution. For $s := kh$ and $t := kL$, let $A_0(s, t)$ be defined in (11). Then, for all $kh \notin \pi\mathbb{Z}$,*

$$(25) \quad k \|u\|_{0,h} \leq A_0(kh, kL) \|f\|_{0,h}, \quad \sqrt{\Theta} |u|_{1,h} \leq A_0(kh, kL) \|f\|_{0,h}.$$

Proof. We use Lemma 8 and Corollary 6. From (22) and (21), we eliminate the H^1 -seminorm to derive

$$(26) \quad (1 + \cos(kh)) \left(k^2 \|u\|_{0,h}^2 + \frac{k^2 h}{2} (|u_0|^2 + |u_n|^2) \right) \leq \frac{L^2}{2\Theta} \|f\|_{0,h}^2 - \cos(kh) \Re(f, u)_h.$$

The Cauchy–Schwarz and Young inequalities with $\varepsilon = 2 \cos^2(kh/2) k^2$ yields

$$(27) \quad |\Re(f, u)_h| \leq \frac{1}{4k^2} \sec^2\left(\frac{kh}{2}\right) \|f\|_{0,h}^2 + \cos^2\left(\frac{kh}{2}\right) k^2 \|u\|_{0,h}^2.$$

Substituting (27) into (26) and dividing by $1 + \cos(kh) = 2 \cos^2(kh/2)$, we obtain

$$k^2 \|u\|_{0,h}^2 \leq \frac{1}{2} \left(\frac{L^2}{2\Theta} \sec^2\left(\frac{kh}{2}\right) + \frac{1}{4k^2} \sec^4\left(\frac{kh}{2}\right) \right) \|f\|_{0,h}^2 + \frac{1}{2} k^2 \|u\|_{0,h}^2,$$

which gives the discrete L^2 -norm estimate in (25). To estimate the discrete H^1 -seminorm, we return to (22) and (21), and eliminate the L^2 -norm to find that

$$(28) \quad \Theta(1 + \cos(kh)) |u|_{1,h}^2 \leq \frac{L^2}{2\Theta} \|f\|_{0,h}^2 + \Re(f, u)_h.$$

Combining (28) with (27), and dividing by $1 + \cos(s) = 2 \cos^2(s/2)$,

$$\Theta |u|_{1,h}^2 \leq \frac{1}{2} \left(\frac{L^2}{2\Theta} \sec^2\left(\frac{kh}{2}\right) + \frac{1}{4k^2} \sec^4\left(\frac{kh}{2}\right) \right) \|f\|_{0,h}^2 + \frac{1}{2} k^2 \|u\|_{0,h}^2.$$

Applying the discrete L^2 estimate in (25) gives the H^1 -seminorm estimate.

It remains to show the well-posedness. If $f \equiv 0$, then (25) implies $u \equiv 0$, so the full discrete problem (14) is unique. Since the BPF discretization defines a square linear system in the finite-dimensional space \mathbb{C}^{n+1} , uniqueness implies existence. Therefore the full discrete problem (14) admits a unique solution, and the proof of Theorem 9 is complete. \square

3.4. Lifting and proof of Theorem 3. We now return to the full BPF discretization (6) with general boundary data $g_0, g_L \in \mathbb{C}$. The key observation is that, by Proposition 2, the homogeneous Helmholtz component generated by the boundary data is reproduced exactly by the BPF scheme. This allows us to reduce the general problem to the homogeneous discrete radiation problem treated in Theorem 9. We begin with a discrete estimate for the exact plane-wave lifting.

Lemma 10 (Plane-wave lifting). *Let*

$$u^{\text{pw}}(x) = \alpha e^{ikx} + \beta e^{-ikx}, \quad \alpha = \frac{g_L}{2ik e^{ikL}}, \quad \beta = -\frac{g_0}{2ik},$$

so that $u^{\text{pw}}(x)$ with $x \in [0, L]$ satisfies the homogeneous Helmholtz equation with impedance boundary data g_0, g_L . Define the sampled grid function $v_i := u^{\text{pw}}(x_i)$ for $i = 0, \dots, n$. Then $v = \{v_i\}_{i=0}^n$ satisfies

$$(29) \quad k \|v\|_{0,h} \leq \frac{\sqrt{L}}{2} (|g_0| + |g_L|), \quad \sqrt{\Theta} |v|_{1,h} \leq \frac{\sqrt{L}}{2} (|g_0| + |g_L|).$$

Proof. For the L^2 bound, we use $|v_i| \leq |\alpha| + |\beta|$ and thus $\|v\|_{0,h}^2 = h \sum_{i=1}^{n-1} |v_i|^2 \leq L (|\alpha| + |\beta|)^2$. The L^2 -norm estimate in (29) then follows from

$$(30) \quad |\alpha| + |\beta| \leq \frac{|g_0| + |g_L|}{2k}.$$

For the discrete H^1 seminorm, we compute for $i = 0, \dots, n-1$,

$$(\nabla_h v)_i = \frac{\alpha(e^{ik(x_i+h)} - e^{ikx_i}) + \beta(e^{-ik(x_i+h)} - e^{-ikx_i})}{h}.$$

Using $|e^{i\theta} - 1| = 2|\sin(\theta/2)|$, we find that

$$|v|_{1,h}^2 = h \sum_{i=0}^{n-1} |(\nabla_h v)_i|^2 \leq \frac{4 \sin^2(kh/2)}{h^2} L (|\alpha| + |\beta|)^2.$$

It follows from (30) and the expression $\Theta(s) = s^2/(4\sin^2(s/2))$ that

$$|v|_{1,h}^2 \leq \frac{L}{4\Theta(kh)} (|g_0| + |g_L|)^2,$$

which is equivalent to the H^1 -seminorm estimate in (29). \square

We now prove the main stability theorem stated at the beginning of this section.

Proof of Theorem 3. Let u_h denote the solution to the BPF scheme (6) with source term f and impedance data g_0, g_L , and let v be the plane-wave lifting constructed in Lemma 10. We deduce from Proposition 2 that

$$D_k^- D_k^+ v = 0, \quad (D_k^+ v)_0 = m(kh)g_0, \quad (D_k^- v)_n = m(kh)g_L.$$

Define the remainder $w := u_h - v$. By linearity of the BPF scheme, w satisfies the BPF scheme (14) with homogeneous radiation conditions. Applying the triangle inequality to $u_h = w + v$ and combining the estimate of w from Theorem 9 and the estimate of v from Lemma 10, we conclude (12) and (13).

It remains to show the well-posedness. The existence of solution u_h is ensured by our construction. If $f \equiv 0$ and $g_0 = g_L = 0$, then (12)–(13) imply $u_h \equiv 0$, so the solution is unique. Therefore the full discrete problem admits a unique solution, and the proof of Theorem 3 is complete. \square

4. CONSISTENCY AND CONVERGENCE

In this section, we establish the consistency of the BPF discretization and derive the corresponding convergence estimates. Let u denote the exact solution of (2)–(3) and let $u_h = \{u_i\}_{i=0}^n$ be the discrete BPF solution to (6). Our goal is to obtain k -explicit second-order bounds for the grid error $e_i := u_i - u(x_i)$ in the discrete L^2 norm and H^1 seminorm.

4.1. Residual equation and main results. We begin by inserting the exact solution into the discrete BPF operator. This gives rise to the interior and boundary residuals that govern the error equation. For the interior nodes $i = 1, \dots, n-1$, we define the interior residual by

$$(31) \quad \tau_i(u) := -\Theta(kh) (\Delta_h u)(x_i) - k^2 u(x_i) - f(x_i).$$

Using the differential equation (2), this can be rewritten equivalently as

$$(32) \quad \tau_i(u) = \Theta(kh) (\Delta_h u)(x_i) - u''(x_i).$$

At the boundary, we define the residuals by

$$(33) \quad \beta_0(u) := \frac{1}{m(kh)} (D_k^+ u)_0 - g_0, \quad \beta_L(u) := \frac{1}{m(kh)} (D_k^- u)_n - g_L.$$

Using Proposition 22 in Appendix A, together with the impedance boundary conditions in (3), we may write them explicitly as

$$(34) \quad \begin{aligned} \beta_0(u) &= \frac{k}{\sin(kh)} \left(u(h) - e^{ikh} u(0) \right) - (u'(0) - iku(0)), \\ \beta_L(u) &= \frac{k}{\sin(kh)} \left(e^{ikh} u(L) - u(L-h) \right) - (u'(L) + iku(L)). \end{aligned}$$

For simplicity, when u is the exact solution to (2)–(3), we omit the arguments:

$$(35) \quad \tau_i := \tau_i(u), \quad \beta_0 := \beta_0(u), \quad \beta_L := \beta_L(u).$$

With these definitions, the grid error satisfies a discrete residual equation of exactly the same form as the BPF scheme.

Lemma 11 (Error equation). *Let u be the exact solution to (2)–(3), and let u_h be the discrete BPF solution to (6). Then the grid error $e_i := u_i - u(x_i)$ for $i = 0, \dots, n$ satisfies*

$$\begin{cases} D_k^- D_k^+ e_i = \tau_i, & i = 1, \dots, n-1, \\ D_k^+ e_0 = m(kh)\beta_0, & D_k^- e_n = m(kh)\beta_L, \end{cases}$$

where τ_i , β_0 , and β_L are given by (32)–(35).

We now state the main results of this section. The first theorem provides k -explicit bounds for the interior and boundary residuals.

Theorem 12 (Consistency and residual bounds). *Assume that $f \in H^3(0, L) \cap H_0^2(0, L)$, and let $\tau = \{\tau_i\}_{i=1}^{n-1}$, β_0 , and β_L be defined by (31) and (33). Then, for any $kh \notin \pi\mathbb{Z}$, the residuals satisfy the second-order estimates*

$$(36) \quad \|\tau\|_{0,h} \leq L \Theta(kh) \frac{h^2}{12} \|f^{(3)}\|_{L^2(0,L)},$$

$$(37) \quad |\beta_0| + |\beta_L| \leq 2\sqrt{L\Theta(kh)} \left| \sec\left(\frac{kh}{2}\right) \right| \frac{h^2}{6} \|f''\|_{L^2(0,L)}.$$

In particular, for any fixed $s_0 < \pi$, the constants in (36)–(37) are uniformly bounded with respect to k whenever $kh \leq s_0$.

Combining the residual equation with the stability result of Theorem 3, we obtain the following convergence theorem.

Theorem 13 (Convergence and error estimate). *Assume that $f \in H^3(0, L) \cap H_0^2(0, L)$. For $s := kh$ and $t := kL$, let $A_0(s, t)$ be defined by (11). Then, for any $kh \notin \pi\mathbb{Z}$, the grid error $e_h = \{e_i\}_{i=0}^n$ satisfies*

$$\begin{aligned} k\|e_h\|_{0,h} &\leq \Theta A_0(kh, kL) \left(L \frac{h^2}{12} \|f^{(3)}\|_{L^2(0,L)} + \frac{h^2}{3} \|f''\|_{L^2(0,L)} \right), \\ \sqrt{\Theta} \|e_h\|_{1,h} &\leq \Theta A_0(kh, kL) \left(L \frac{h^2}{12} \|f^{(3)}\|_{L^2(0,L)} + \frac{h^2}{3} \|f''\|_{L^2(0,L)} \right). \end{aligned}$$

In particular, for $s_0 < \pi$, the method is second-order convergent in $\|\cdot\|_{0,h}$ and $|\cdot|_{1,h}$, with constants uniformly bounded with respect to k whenever $kh \leq s_0$ and $kL \geq \pi$.

The remainder of this section is devoted to proving the k -explicit consistency estimates stated in Theorem 12. As a Taylor expansion of the leading interior and boundary consistency terms does not provide a k -uniform control of the remainders, we choose a Fourier-based approach inspired by [16]. In the present setting, the impedance boundary closures introduce additional difficulties, which are overcome by lifting the Helmholtz kernel component.

4.2. Exact kernel lifting and sine expansion. We begin the proof of Theorem 12. The key observation is that the BPF discretization is exact on the Helmholtz kernel span $\{e^{\pm ikx}\}$. This allows us to separate from the exact solution a homogeneous oscillatory component that contributes no residual, and to reduce the consistency analysis to a zero-trace remainder.

Lemma 14 (Exact kernel lifting). *Assume that $\sin(kL) \neq 0$. Then there exists a unique function $b \in C^\infty([0, L])$ such that*

$$(38) \quad -b'' - k^2b = 0 \quad \text{in } (0, L), \quad b(0) = u(0), \quad b(L) = u(L).$$

Moreover, b belongs to $\text{span}\{\cos(kx), \sin(kx)\} = \text{span}\{e^{\pm ikx}\}$.

Proof. The general solution to the homogeneous Helmholtz equation $-b'' - k^2b = 0$ is of the form $b(x) = A \cos(kx) + B \sin(kx)$ with $A, B \in \mathbb{C}$. The boundary conditions in (38) give $A = u(0)$ and $A \cos(kL) + B \sin(kL) = u(L)$. Since $\sin(kL) \neq 0$, this system is nonsingular and therefore determines a unique pair (A, B) . The representation above also shows that $b \in \text{span}\{\cos(kx), \sin(kx)\}$. \square

Remark 15 (Resonant wavenumbers). *The assumption $\sin(kL) \neq 0$ is imposed only to simplify the derivation. If $\sin(kL) = 0$ (i.e. $kL = n\pi$ for some integer n), one may apply a limiting procedure. The residual estimates obtained below extend to the resonant case $\sin(kL) = 0$ by continuity with respect to k .*

We now define the lifted remainder $w := u - b$. Since u solves (2) and b satisfies (38), it follows that $w(0) = u(0) - b(0) = 0$ and $w(L) = u(L) - b(L) = 0$. Then, the lifted remainder w satisfies the Dirichlet problem

$$(39) \quad -w'' - k^2w = f \quad \text{in } (0, L), \quad w(0) = w(L) = 0.$$

The relevance of this decomposition is that the kernel part b produces no truncation error. Indeed, by Proposition 2, the BPF scheme is exact on the plane waves $e^{\pm ikx}$ and hence, by linearity, on the entire space $\text{span}\{e^{\pm ikx}\}$. Therefore, $\tau_i(b) = 0$ for $i = 1, \dots, n-1$ and $\beta_0(b) = 0, \beta_L(b) = 0$. The residuals of the exact solution reduce to those of the lifted remainder:

$$\tau_i(u) = \tau_i(w), \quad i = 1, \dots, n-1, \quad \beta_0(u) = \beta_0(w), \quad \beta_L(u) = \beta_L(w).$$

Since $w(0) = w(L) = 0$, the boundary residuals (34)-(35) admit the simplified forms

$$(40) \quad \beta_0 = \beta_0(w) = \frac{k}{\sin(kh)} w(h) - w'(0),$$

$$(41) \quad \beta_L = \beta_L(w) = \frac{-k}{\sin(kh)} w(L-h) - w'(L).$$

Thus, the truncation errors are determined by the zero-trace solution w of (39).

To expand the lifted zero-trace component w in the sine basis, we introduce

$$(42) \quad \phi_n(x) := \sqrt{\frac{2}{L}} \sin(\xi_n x), \quad \xi_n := \frac{n\pi}{L}, \quad n \in \mathbb{N}.$$

Then $\{\phi_n\}_{n \geq 1}$ is an orthonormal basis of $L^2(0, L)$, and

$$(43) \quad w(x) = \sum_{n \geq 1} \widehat{w}_n \phi_n(x), \quad \widehat{w}_n := (w, \phi_n)_{L^2(0, L)}.$$

Similarly, since $f \in L^2(0, L)$, we may write

$$f(x) = \sum_{n \geq 1} \widehat{f}_n \phi_n(x), \quad \widehat{f}_n := (f, \phi_n)_{L^2(0, L)}.$$

In the next two subsections, we use the Fourier-based analysis to derive separate k -explicit estimates for the interior residual τ and the boundary residuals β_0 and β_L .

4.3. Interior residual estimate. We estimate the interior residual $\tau_i(w)$ by adopting a “semi-discrete” viewpoint. For this, we introduce the continuous and semi-discrete Helmholtz operators on $C^2[0, L]$:

$$(44) \quad \mathcal{L} := -\partial_{xx} - k^2, \quad \mathcal{L}_h := -\Theta(kh) \Delta_h - k^2.$$

Then the interior truncation error (32) can be extended to a pointwise residual,

$$(45) \quad \tau_h(x) := (\mathcal{L}_h - \mathcal{L})w(x), \quad x \in (0, L),$$

so that, by construction,

$$(46) \quad \tau_i(w) = \tau_i(u) = \tau_h(x_i), \quad i = 1, \dots, n-1.$$

By (46), it suffices to analyze the pointwise residual $\tau_h(x)$. We use Fourier multiplier analysis. Note that the sine basis diagonalizes the continuous and semi-discrete Helmholtz operators. Indeed, from (42),

$$(47) \quad \mathcal{L}\phi_n = (-\phi_n'' - k^2\phi_n) = (\xi_n^2 - k^2)\phi_n =: \lambda(\xi_n)\phi_n.$$

Moreover, since

$$(\Delta_h \phi_n)(x) = -\frac{4}{h^2} \sin^2\left(\frac{\xi_n h}{2}\right) \phi_n(x),$$

it follows from (44) that

$$(48) \quad \mathcal{L}_h \phi_n = \left(\Theta(kh) \frac{4}{h^2} \sin^2\left(\frac{\xi_n h}{2}\right) - k^2 \right) \phi_n =: \widetilde{\lambda}_h(\xi_n) \phi_n.$$

Finally, testing the Helmholtz equation (39) with ϕ_n gives the modal relation

$$(49) \quad \lambda(\xi_n) \widehat{w}_n = \widehat{f}_n, \quad \text{that is,} \quad \widehat{w}_n = \frac{\widehat{f}_n}{\lambda(\xi_n)}, \quad n \geq 1.$$

We begin with the modal representation of $\tau_h(x)$ in the sine basis.

Lemma 16 (Modal representation of the interior residual). *Let u be the exact solution to (2)–(3), let b and $w = u - b$ be defined as in Section 4.2, and let τ_h be given by (45). Then*

$$\tau_h(x) = \sum_{n \geq 1} \widehat{\tau}_{h,n} \phi_n(x),$$

where for $n \geq 1$,

$$(50) \quad \widehat{\tau}_{h,n} = M_h(\xi_n; h, k) \widehat{f}_n,$$

$$(51) \quad M_h(\xi; h, k) := \frac{\widetilde{\lambda}_h(\xi) - \lambda(\xi)}{\lambda(\xi)} = \frac{\Theta(kh) \frac{4}{h^2} \sin^2\left(\frac{\xi h}{2}\right) - \xi^2}{\xi^2 - k^2}.$$

Here, $\lambda(\xi)$ and $\widetilde{\lambda}_h(\xi)$ are the Fourier symbols of \mathcal{L} and \mathcal{L}_h defined in (47) and (48), respectively.

Proof. It follows from definition (45) of τ_h and expansion (43) of w that

$$\tau_h = (\mathcal{L}_h - \mathcal{L})w = \sum_{n \geq 1} \widehat{w}_n (\mathcal{L}_h - \mathcal{L})\phi_n = \sum_{n \geq 1} \widehat{w}_n (\widetilde{\lambda}_h(\xi_n) - \lambda(\xi_n))\phi_n,$$

where we used (47) and (48) in the last line. We apply (49) to obtain

$$\widehat{\tau}_{h,n} = (\widetilde{\lambda}_h(\xi_n) - \lambda(\xi_n))\widehat{w}_n = \frac{\widetilde{\lambda}_h(\xi_n) - \lambda(\xi_n)}{\lambda(\xi_n)} \widehat{f}_n,$$

which is exactly (50)–(51). □

The next lemma gives a k -explicit bound for the multiplier M_h .

Lemma 17 (Uniform bound for the interior multiplier). *It holds for all $kh \notin \pi\mathbb{Z}$ and $\xi > 0$ that*

$$(52) \quad |M_h(\xi; h, k)| \leq \Theta(kh) \frac{h^2}{12} \xi^2.$$

Proof. Set $A := \xi h/2$ and $B := kh/2$. The multiplier (51) can be rewritten as

$$M_h(\xi; h, k) = \frac{\Theta \sin^2 A - A^2}{A^2 - B^2}.$$

Introducing the function $g(t) := \sin^2(\sqrt{t})/t$ for $t > 0$, we have $\sin^2 A = A^2 g(A^2)$ and $\sin^2 B = B^2 g(B^2)$. Then, in view of $\Theta = 1/g(B^2)$ and the mean value theorem,

$$|M_h(\xi; h, k)| = \left| A^2 \Theta(kh) \frac{g(A^2) - g(B^2)}{A^2 - B^2} \right| \leq A^2 \Theta(kh) \sup_{t > 0} |g'(t)|.$$

We refer to the Appendix for a proof that $\sup_{t>0} |g'(t)| \leq 1/3$. Hence

$$|M_h(\xi; h, k)| \leq A^2 \Theta(kh) \cdot \frac{1}{3} = \Theta(kh) \frac{h^2}{12} \xi^2,$$

which proves (52). \square

We can now derive the k -explicit bound for the interior residual.

Theorem 18 (Interior residual estimate). *Assume that $f \in H^3(0, L) \cap H_0^2(0, L)$. Then the interior residual $\tau = \{\tau_i\}_{i=1}^{n-1}$ satisfies*

$$(53) \quad \|\tau\|_{0,h} \leq L \Theta(kh) \frac{h^2}{12} \|f^{(3)}\|_{L^2(0,L)},$$

so the interior part of Theorem 12 follows. Moreover, under the fixed-resolution condition $kh \leq s_0 < \pi$, the constant in (53) is uniformly bounded with respect to k .

Proof. We know from Lemma 16 that

$$\tau_h(x) = \sum_{n \geq 1} M_h(\xi_n; h, k) \widehat{f}_n \phi_n(x).$$

Using $|\phi_n(x)| \leq \sqrt{2/L}$ and the Cauchy–Schwarz inequality, we obtain

$$\begin{aligned} |\tau_h(x)| &\leq \sqrt{\frac{2}{L}} \sum_{n \geq 1} |M_h(\xi_n; h, k)| |\widehat{f}_n| \\ &\leq \sqrt{\frac{2}{L}} \left(\sum_{n \geq 1} |M_h(\xi_n; h, k)|^2 \xi_n^{-6} \right)^{1/2} \left(\sum_{n \geq 1} \xi_n^6 |\widehat{f}_n|^2 \right)^{1/2}. \end{aligned}$$

By Lemma 17,

$$\sum_{n \geq 1} |M_h(\xi_n; h, k)|^2 \xi_n^{-6} \leq \Theta(kh)^2 \frac{h^4}{144} \sum_{n \geq 1} \xi_n^{-2}.$$

Since $\xi_n = n\pi/L$,

$$(54) \quad \sum_{n \geq 1} \xi_n^{-2} = \frac{L^2}{\pi^2} \sum_{n \geq 1} \frac{1}{n^2} = \frac{L^2}{6}.$$

Because of $f \in H^3(0, L) \cap H_0^2(0, L)$, Parseval's identity for the sine basis gives $\sum_{n \geq 1} \xi_n^6 |\widehat{f}_n|^2 = \|f^{(3)}\|_{L^2(0,L)}^2$. Combining these estimates, we find that

$$|\tau_h(x)| \leq \sqrt{\frac{2}{L}} \frac{\Theta(kh) h^2}{12} \left(\frac{L^2}{6} \right)^{1/2} \|f^{(3)}\|_{L^2(0,L)} = \sqrt{\frac{L}{3}} \frac{\Theta(kh) h^2}{12} \|f^{(3)}\|_{L^2(0,L)}.$$

Finally, using (46),

$$\|\tau\|_{0,h} = \left(h \sum_{i=1}^{n-1} |\tau_h(x_i)|^2 \right)^{1/2} \leq \sqrt{L} \|\tau_h\|_{L^\infty(0,L)} \leq \frac{L \Theta(kh)}{12\sqrt{3}} h^2 \|f^{(3)}\|_{L^2(0,L)}.$$

This proves (53). \square

4.4. Boundary residual estimate. We turn to the boundary residuals β_0, β_L , which are defined in (34)–(35). We first derive their modal representation.

Lemma 19 (Modal representation of the boundary residuals). *Let u be the exact solution to (2)–(3), let $w = u - b$, where b is defined in Lemma 14, and let β_0, β_L be defined by (40)–(41). Then*

$$(55) \quad \beta_0 = \sum_{n \geq 1} B_h(\xi_n; h, k) \widehat{f}_n, \quad \beta_L = \sum_{n \geq 1} (-1)^n B_h(\xi_n; h, k) \widehat{f}_n, \quad \text{where}$$

$$B_h(\xi; h, k) = \sqrt{\frac{2}{L}} \frac{h}{\sin(kh)} \frac{kh \sin(\xi h) - \xi h \sin(kh)}{(\xi h)^2 - (kh)^2}.$$

Proof. We infer from expansion (43) of w in the sine basis that

$$w'(0) = \sum_{n \geq 1} \sqrt{\frac{2}{L}} \xi_n \widehat{w}_n, \quad w(h) = \sum_{n \geq 1} \sqrt{\frac{2}{L}} \sin(\xi_n h) \widehat{w}_n.$$

Since (49) gives $(\xi_n^2 - k^2) \widehat{w}_n = \widehat{f}_n$, we deduce from (40) that

$$\begin{aligned} \beta_0 &= \sum_{n \geq 1} \sqrt{\frac{2}{L}} \left(\frac{k}{\sin(kh)} \sin(\xi_n h) - \xi_n \right) \widehat{w}_n \\ &= \sum_{n \geq 1} \sqrt{\frac{2}{L}} \frac{\frac{k}{\sin(kh)} \sin(\xi_n h) - \xi_n}{\xi_n^2 - k^2} \widehat{f}_n = \sum_{n \geq 1} B_h(\xi_n; h, k) \widehat{f}_n. \end{aligned}$$

For the right endpoint, we use $\sin(\xi_n L) = 0$ and $\cos(\xi_n L) = (-1)^n$ to write

$$\begin{aligned} w'(L) &= \sum_{n \geq 1} \sqrt{\frac{2}{L}} (-1)^n \xi_n \widehat{w}_n, \\ w(L-h) &= \sum_{n \geq 1} \sqrt{\frac{2}{L}} \sin(\xi_n(L-h)) \widehat{w}_n = - \sum_{n \geq 1} \sqrt{\frac{2}{L}} (-1)^n \sin(\xi_n h) \widehat{w}_n, \end{aligned}$$

where we have used $\sin(a-b) = \sin(a) \cos(b) - \cos(a) \sin(b)$ in the last equality. Substituting into (41), we obtain

$$\beta_L = \sum_{n \geq 1} \sqrt{\frac{2}{L}} (-1)^n \left(\frac{k}{\sin(kh)} \sin(\xi_n h) - \xi_n \right) \widehat{w}_n = \sum_{n \geq 1} (-1)^n B_h(\xi_n; h, k) \widehat{f}_n,$$

which finishes the proof. \square

The next lemma gives a k -explicit bound for the boundary multiplier.

Lemma 20 (Uniform bound for the boundary multiplier). *It holds for all $kh \notin \pi\mathbb{Z}$ and $\xi > 0$ that*

$$|B_h(\xi; h, k)| \leq \sqrt{\frac{2\Theta(kh)}{L}} \frac{\xi h^2}{6} \left| \sec\left(\frac{kh}{2}\right) \right|.$$

Proof. Starting from (55), we rewrite B_h as

$$B_h(\xi; h, k) = \sqrt{\frac{2}{L}} \frac{hAB}{\sin B} \frac{h(A^2) - h(B^2)}{A^2 - B^2}, \quad A := \xi h, \quad B := kh,$$

where $h(t) := \sin(\sqrt{t})/\sqrt{t}$ for $t > 0$. We apply the mean-value theorem and the bound $\sup_{t>0} |h'(t)| \leq 1/6$ from Lemma 23 in the Appendix:

$$\begin{aligned} |B_h(\xi; h, k)| &\leq \sqrt{\frac{2}{L}} \frac{hAB}{|\sin B|} \sup_{t>0} |h'(t)| \leq \sqrt{\frac{2}{L}} \frac{\xi h^2}{6} \frac{kh}{|\sin(kh)|} \\ &= \sqrt{\frac{2}{L}} \frac{\xi h^2}{6} \sqrt{\Theta(kh)} \left| \sec\left(\frac{kh}{2}\right) \right|. \end{aligned}$$

This ends the proof. □

We can now estimate the boundary residuals.

Theorem 21 (Boundary residual estimate). *Assume that $f \in H_0^2(0, L)$. Then*

$$(56) \quad |\beta_0| + |\beta_L| \leq 2\sqrt{L\Theta(kh)} \left| \sec\left(\frac{kh}{2}\right) \right| \frac{h^2}{6} \|f''\|_{L^2(0,L)},$$

so the boundary part of Theorem 12 follows. Moreover, under the fixed-resolution condition $kh \leq s_0 < \pi$, the constant in (56) is uniformly bounded with respect to k .

Proof. We conclude from Lemma 19 and the Cauchy–Schwarz inequality that

$$|\beta_0| = \left| \sum_{n \geq 1} B_h(\xi_n; h, k) \widehat{f}_n \right| \leq \left(\sum_{n \geq 1} |B_h(\xi_n; h, k)|^2 \xi_n^{-4} \right)^{1/2} \left(\sum_{n \geq 1} \xi_n^4 |\widehat{f}_n|^2 \right)^{1/2}.$$

It follows from Lemma 20 and (54) that

$$\sum_{n \geq 1} |B_h(\xi_n; h, k)|^2 \xi_n^{-4} \leq \frac{2\Theta}{L} \sec^2\left(\frac{kh}{2}\right) \frac{h^4}{36} \sum_{n \geq 1} \xi_n^{-2} = \frac{L\Theta}{3} \sec^2\left(\frac{kh}{2}\right) \frac{h^4}{36}.$$

Moreover, because of $f \in H_0^2(0, L)$, Parseval's identity for the sine basis yields $\sum_{n \geq 1} \xi_n^4 |\widehat{f}_n|^2 = \|f''\|_{L^2(0,L)}^2$. Combining these estimates, we obtain

$$(57) \quad |\beta_0| \leq \left(\frac{L\Theta}{3} \sec^2\left(\frac{kh}{2}\right) \frac{h^4}{36} \right)^{1/2} \|f''\|_{L^2(0,L)}.$$

For the right endpoint, Lemma 19 shows that $|\widetilde{B}_h(\xi_n; h, k)| = |B_h(\xi_n; h, k)|$ and thus, the same argument yields the same bound as in (57). Finally, summing the estimates of β_0 and β_L leads to (56). □

5. NUMERICAL EXPERIMENT

In this section, we present numerical experiments for the proposed BPF scheme. The first two tests are designed to validate the theoretical analysis. We then test the robustness of the BPF scheme in terms of nonsmooth sources. Finally, we compare various numerical methods.

We consider the relative L^∞ - and V -errors, defined by, respectively,

$$\|e\|_{L^\infty} = \frac{\|u - u_h\|_{L^\infty}}{\|u\|_{L^\infty}}, \quad \|e\|_V = \frac{\|u - u_h\|_V}{\|u\|_V},$$

where $\|u\|_V^2 = k^2\|u\|_{0,h}^2 + |u|_{1,h}^2$, and u is the reference solution.

5.1. Exact resolution of a 1D plane wave. As shown in Section 2.4, the BPF scheme exactly reproduces plane-wave solutions. To illustrate this property, we consider the exact $u(x) = 2e^{ikx} + e^{-ikx}$ over the interval $(0, 1)$. The corresponding impedance are $g_0 = u'(0) - iku(0) = -2ik$ and $g_1 = u'(1) + iku(1) = 4ike^{ik}$. We choose the wavenumber $k = 2^7$ and the coarse mesh size $h = 2^{-3}$. With this setup, the computed solution agrees with the sampled exact solution up to machine precision; more precisely, the absolute L^∞ -error is 2.91×10^{-15} . In Figure 1, we plot the real and imaginary parts of the exact and numerical solutions. The figure shows that the BPF scheme reproduces the plane wave accurately even on a very coarse mesh.

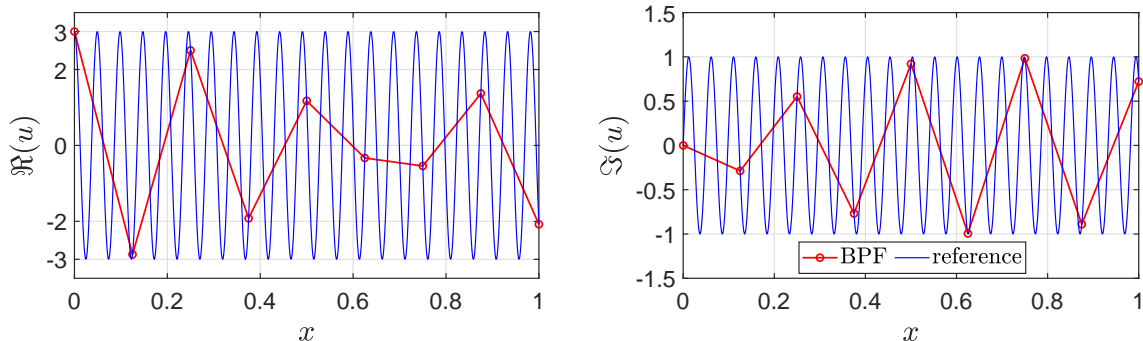


FIGURE 1. Comparison between the reference solution and the numerical solution for the plane-wave test on a coarse mesh.

5.2. A smooth manufactured-solution test. To directly validate the convergence estimate of Theorem 4.3, we consider the smooth manufactured solution $u(x) = e^{ikx} + r(x)$, $r(x) := x^4(1-x)^4$ for $x \in (0, 1)$. The source term is defined by $f(x) = r''(x) + k^2r(x)$ or, more explicitly,

$$f(x) = 12x^2(1-x)^4 - 32x^3(1-x)^3 + 12x^4(1-x)^2 + k^2x^4(1-x)^4.$$

The impedance boundary data are taken from the exact solution:

$$g_0 = u'(0) - iku(0) = 0, \quad g_1 = u'(1) + iku(1) = 2ike^{ik}.$$

Taking into account that r has fourth-order zeros at both endpoints, it follows that $f(0) = f(1) = f'(0) = f'(1) = 0$, so this example is consistent with our regularity assumptions. Moreover, it holds that $\|f^{(\alpha)}\|_2 \lesssim k^2$ for $\alpha = 2, 3$.

We report the relative L^∞ - and V -errors as the mesh is refined with $h = 3^{-9}, \dots, 3^{-5}$. Because the V -norm of the exact solution does not depend on h when k is fixed, the relative V -norm error is the same as the absolute energy error when assessing the convergence rate in relation to h . Figure 2 shows that the BPF solution exhibits second-order convergence under mesh refinement, in agreement with Theorem 4.3.

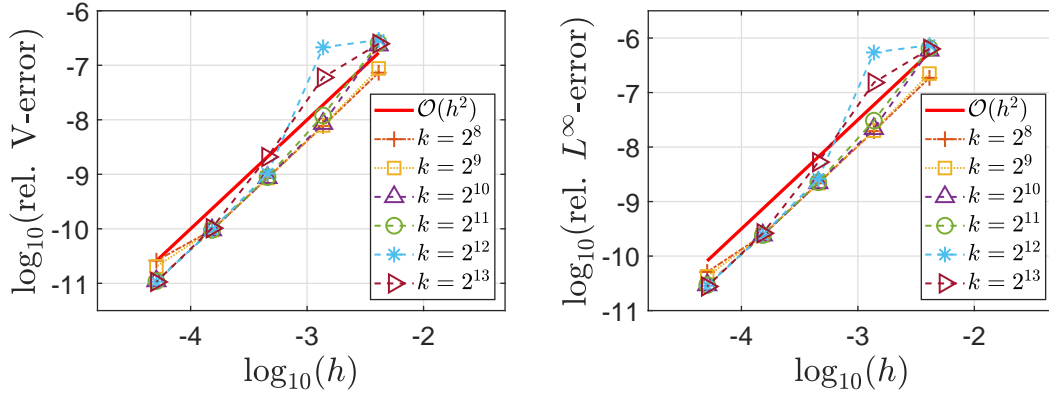


FIGURE 2. Results for the smooth-source test: convergence with respect to h in the relative V -norm (left) and the relative L^∞ -norm (right).

5.3. A nonsmooth-source test. We consider a nonsmooth source term to illustrate the robustness of the BPF scheme beyond the regularity assumptions required in Theorem 4.3. We take $f(x) = 50$ for $|x - 0.5| \leq 1/9$ and $f(x) = 0$ else, together with the nonhomogeneous impedance boundary condition

$$(58) \quad u'(0) - iku(0) = 2, \quad u'(1) + iku(1) = i.$$

Since an exact solution is not available, we compute a reference solution on the fine mesh $h = 3^{-12}$. This example does not satisfy the smoothness assumptions of the theoretical analysis. We choose $h = 3^{-10}, \dots, 3^{-5}$. As shown in Figure 3, the BPF scheme still exhibits an approximately second-order convergence trend with respect to h in the relative V - and L^∞ -norms, despite the low regularity of the source term.

5.4. Fixed-resolution behavior. The resolution condition plays a fundamental role in the numerical simulation of highly oscillatory Helmholtz problems. In particular, it is closely related to pollution effects and on the number of grid points per wavelength. We therefore examine the behavior of the BPF scheme for varying values of k and h , and compare it with the classical finite difference (FD) method and the dispersion-corrected FD method [7].

We consider the problem with source term $f(x) = \sin^2(\pi x)$, together with the impedance boundary condition (58). Then $f \in H^3(0, L) \cap H_0^2(0, L)$ satisfies the assumption of Theorem

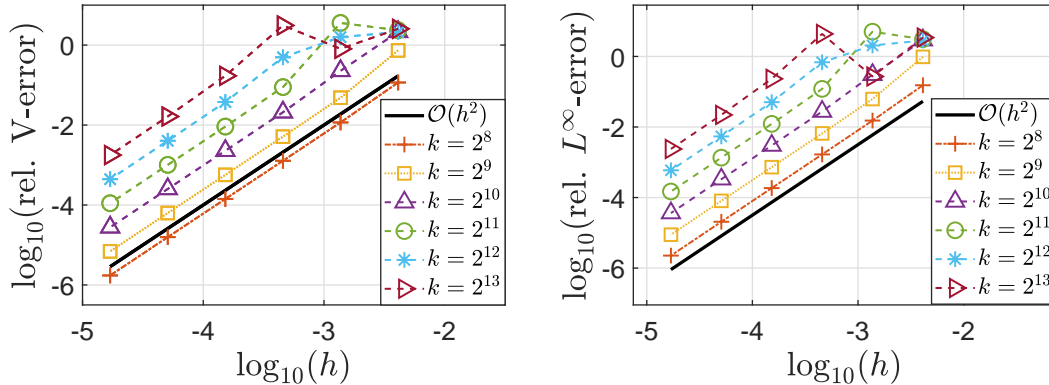


FIGURE 3. Results for the nonsmooth-source test: convergence with respect to h in the relative V -norm (left) and the relative L^∞ -norm (right)

4.3. The reference solution is computed on the fine mesh $h = 2^{-18}$. For the present benchmark, the numerical data indicate that $\|u\|_{L^\infty}$ and $\|u\|_{L^2}$ scale like k^{-1} , whereas the discrete energy norm $\|u\|_V$ is nearly independent of k . We therefore use the relative V -norm error as the main quantity. For the comparison plots, we instead use the relative L^∞ -error, which provides a direct pointwise measure of accuracy and gives a clear visual comparison between the three methods.

Table 1 reports the relative V -norm error of the BPF scheme for different values of k and h . The table contains two types of information. Along each row, the error decreases by approximately a factor of four when h is halved, indicating a second-order convergence trend for fixed k . Along each parallel diagonal, the quantity kh is fixed, or equivalently, the number of grid points per wavelength $\text{PPW} = 2\pi/(kh)$ is fixed. Along these diagonals, the error decreases steadily as k increases, which confirms the $O(k^{-2})$ decay predicted by the second-order convergence estimate under fixed resolution. In the present example, the observed decay is in fact empirically faster than this theoretical rate. The table also contains values outside the principal Nyquist regime $0 < kh < \pi$; these are still covered by the general theory, since the main estimates hold for all $kh \notin \pi\mathbb{Z}$. For example, when $k = 2^{10}$ and $h = 2^{-5}$, so that $kh = 32$, the relative V -norm error is still only 4.08×10^{-5} in this benchmark.

When the classical finite difference (FD) method is used, increasingly fine meshes are required for large wavenumbers because of the well-known dispersion pollution effect. A dispersion-corrected FD method was proposed in [7] to alleviate this difficulty; in that approach, the error is primarily governed by the quantity kh , so that reasonable accuracy may still be obtained when the resolution is chosen appropriately. Figure 4 provides a direct visual comparison of the three methods, all evaluated at fixed values of kh . It shows that the classical FD error deteriorates rapidly as k increases, while the dispersion-corrected FD method improves this behavior but still remains significantly less accurate than the BPF method over the tested parameter range. By contrast, the BPF scheme consistently produces the smallest errors, confirming its clear advantage in this benchmark. As in the

TABLE 1. Relative V -norm error of the BPF scheme for different values of k and h . Parallel diagonals correspond to fixed values of kh , or equivalently, fixed numbers of grid points per wavelength.

$k \backslash h$	2^{-5}	2^{-6}	2^{-7}	2^{-8}	2^{-9}	2^{-10}
2^5	4.18e-05	1.01e-05	2.52e-06	6.27e-07	1.56e-07	3.85e-08
2^6	2.29e-05	5.05e-06	1.22e-06	2.96e-07	6.82e-08	1.81e-08
2^7	2.48e-05	2.86e-06	6.26e-07	1.49e-07	3.41e-08	9.85e-09
2^8	2.10e-05	3.00e-06	3.64e-07	8.45e-08	2.58e-08	1.31e-08
2^9	6.16e-06	2.55e-06	3.76e-07	4.36e-08	8.83e-09	2.24e-09
2^{10}	4.08e-05	7.51e-07	3.16e-07	4.64e-08	5.08e-09	1.24e-09

relative V -norm data, the relative L^∞ -error also shows an empirically faster decay than the $O(k^{-2})$ behavior guaranteed by our theory, with an apparent rate close to third order in this benchmark.

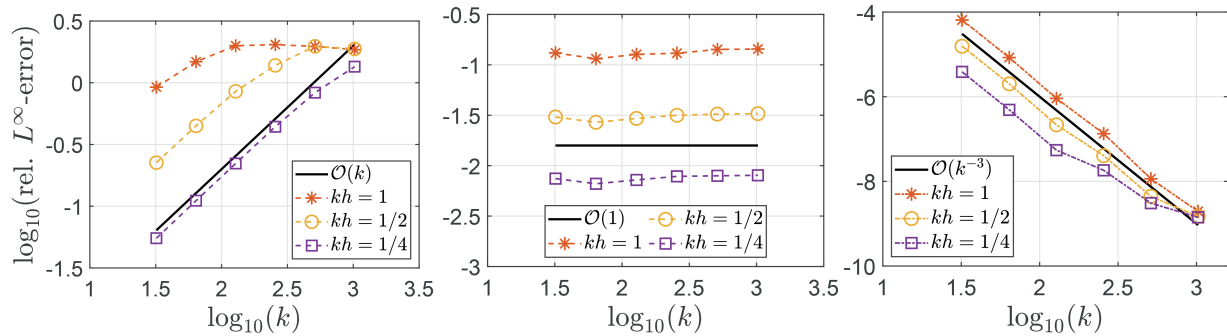


FIGURE 4. Relative L^∞ -error versus k for the classical FD method (left), dispersion-corrected FD method (middle), and BPF scheme evaluated at fixed values of kh (right).

6. CONCLUSION AND OUTLOOK

In this paper, we introduced a Bernoulli phase-fitted scheme for the one-dimensional Helmholtz equation with impedance boundary conditions. The scheme is derived from a complexified Scharfetter–Gummel discretization of the one-way factorization of the Helmholtz operator. For the homogeneous problem, the scheme reproduces the sampled plane-wave solutions exactly, both in the interior and at the discrete impedance boundary closures. For the inhomogeneous problem, we established well-posedness, derived wavenumber-explicit stability estimates, and proved second-order consistency and convergence. These results hold more generally for $kh \notin \pi\mathbb{Z}$, and in particular yield a pollution-free convergence theory for fixed resolution within the principal Nyquist regime. The numerical experiments

demonstrate the favorable fixed-resolution behavior of the BPF scheme in comparison with standard and dispersion-corrected finite difference methods.

A natural next step is the extension of the present factorization-based framework to multidimensional and higher-order discretizations. We found that the factorized 5-point discretization reproduces the tested two-dimensional plane-wave data very accurately. A detailed analysis is deferred to future work.

APPENDIX A. AUXILIARY RESULTS

We prove some results used in this paper.

Proposition 22. *For $i \in \mathcal{I}_h$, the interior scheme in (6) can be written as*

$$D_k^- D_k^+ u_i = \Theta(kh) \frac{u_{i+1} - 2u_i + u_{i-1}}{h^2} + k^2 u_i,$$

and the boundary conditions in (6) are equivalent to

$$(59) \quad \begin{aligned} \frac{1}{m(kh)} D_k^+ u_0 &= \frac{k}{\sin(kh)} (u_1 - e^{ikh} u_0), \\ \frac{1}{m(kh)} D_k^- u_n &= \frac{k}{\sin(kh)} (e^{ikh} u_n - u_{n-1}), \end{aligned}$$

where $m(s) = e^{-is/2} \cos(s/2)$ for $s > 0$.

Proof. A direct calculation shows that

$$(60) \quad \begin{aligned} D_k^- D_k^+ u_i &= \frac{1}{h} (B(ikh) D_k^- u_{i+1} - B(-ikh) D_k^- u_i) \\ &= \frac{1}{h^2} (\Theta(kh) u_{i+1} - (B^2(ikh) + B^2(-ikh)) u_i + \Theta(kh) u_{i-1}) \end{aligned}$$

We deduce from (5) that

$$\begin{aligned} B^2(ikh) + B^2(-ikh) &= (B(ikh) - B(-ikh))^2 + 2B(ikh)B(-ikh) \\ &= -k^2 h^2 + 2\Theta(kh). \end{aligned}$$

A substitution into (60) leads to the interior formula. For the boundary condition, we apply identity (5) again to find that

$$(61) \quad D_k^+ u_0 = \frac{1}{h} (B(ikh) u_1 - B(-ikh) u_0) = \frac{B(ikh)}{h} (u_1 - e^{ikh} u_0).$$

It follows from the definition of $m(s)$ and $2 \sin(s/2) \cos(s/2) = \sin(s)$ that

$$(62) \quad B(is) = \frac{is}{e^{is} - 1} = \frac{se^{-is/2}}{2 \sin(s/2)}, \quad \text{so} \quad \frac{B(is)}{m(s)} = \frac{s}{\sin(s)}.$$

Using this identity into (61) leads to the first formula in (59). The second formula in (59) can be derived similarly. \square

Lemma 23. Let $g(t) := \sin^2(\sqrt{t})/t$ and $h(t) := \sqrt{g(t)} = \sin(\sqrt{t})/\sqrt{t}$ for $t > 0$. Then $g, h \in C^1(0, \infty)$ and

$$(63) \quad \sup_{t>0} |g'(t)| \leq \frac{1}{3}, \quad \sup_{t>0} |h'(t)| \leq \frac{1}{6}.$$

Proof. We first estimate $h'(t)$. For $t > 0$, write $t = s^2$ with $s > 0$. Then

$$h'(t) = \frac{1}{2s} \frac{d}{ds} \left(\frac{\sin s}{s} \right) = \frac{s \cos s - \sin s}{2s^3},$$

and the identity $\sin s - s \cos s = \int_0^s r \sin r \, dr$ yields the estimate

$$|h'(t)| \leq \frac{1}{2s^3} \int_0^s r |\sin r| \, dr \leq \frac{1}{2s^3} \int_0^s r^2 \, dr = \frac{1}{2s^3} \cdot \frac{s^3}{3} = \frac{1}{6}.$$

Finally, since $h(t) \leq 1$, we have $|g'(t)| \leq 2h(t)|h'(t)| \leq 1/3$. This proves (63). \square

REFERENCES

- [1] I. M. BABUŠKA AND S. A. SAUTER, *Is the pollution effect of the FEM avoidable for the Helmholtz equation considering high wave numbers?*, SIAM J. Numer. Anal., 34 (1997), pp. 2392–2423.
- [2] A. BAYLISS, C. I. GOLDSTEIN, AND E. TURKEL, *On accuracy conditions for the numerical computation of waves*, J. Comput. Phys., 59 (1985), pp. 396–404.
- [3] M. BESSEMOULIN-CHATARD, *A finite volume scheme for convection-diffusion equations with nonlinear diffusion derived from the Scharfetter–Gummel scheme*, Numer. Math., 121 (2012), pp. 637–670.
- [4] O. CESSENAT AND B. DESPRES, *Application of an ultra weak variational formulation of elliptic PDEs to the two-dimensional Helmholtz problem*, SIAM J. Numer. Anal., 35 (1998), pp. 255–299.
- [5] Z. CHEN, D. CHENG, AND T. WU, *A dispersion minimizing finite difference scheme and preconditioned solver for the 3D Helmholtz equation*, J. Comput. Phys., 231 (2012), pp. 8152–8175.
- [6] D. CHENG, X. TAN, AND T. ZENG, *A dispersion minimizing finite difference scheme for the Helmholtz equation based on point-weighting*, Comput. Math. Appl., 73 (2017), pp. 2345–2359.
- [7] P.-H. COCQUET AND M. J. GANDER, *Asymptotic dispersion correction in general finite difference schemes for Helmholtz problems*, SIAM J. Sci. Comput., 46 (2024), pp. A670–A696.
- [8] P.-H. COCQUET, M. J. GANDER, AND X. XIANG, *A finite difference method with optimized dispersion correction for the Helmholtz equation*, in International Conference on Domain Decomposition Methods, Springer, 2017, pp. 205–213.
- [9] P.-H. COCQUET, M. J. GANDER, AND X. XIANG, *Closed form dispersion corrections including a real shifted wavenumber for finite difference discretizations of 2D constant coefficient Helmholtz problems*, SIAM J. Sci. Comput., 43 (2021), pp. A278–A308.
- [10] H. DASTOUR AND W. LIAO, *A generalized optimal fourth-order finite difference scheme for a 2D Helmholtz equation with the perfectly matched layer boundary condition*, J. Comput. Appl. Math., 394 (2021), p. 113544.
- [11] H. DASTOUR AND W. LIAO, *An optimal 13-point finite difference scheme for a 2D Helmholtz equation with a perfectly matched layer boundary condition*, Numer. Algor., 86 (2021), pp. 1109–1141.
- [12] A. DERAEMAEKER, I. BABUŠKA, AND P. BOUILLARD, *Dispersion and pollution of the FEM solution for the Helmholtz equation in one, two and three dimensions*, Int. J. Numer. Meth. Engin., 46 (1999), pp. 471–499.
- [13] O. G. ERNST AND M. J. GANDER, *Multigrid methods for Helmholtz problems: A convergent scheme in 1D using standard components*, in Direct and Inverse Problems in Wave Propagation and Applications, I. G. Graham, U. Langer, J. M. Melenk, and M. Sini, eds., De Gruyter, 2013, pp. 135–186.

- [14] X. FENG AND H. WU, *hp-discontinuous Galerkin methods for the Helmholtz equation with large wave number*, Math. Comput., 80 (2011), pp. 1997–2024.
- [15] J. GALKOWSKI AND E. A. SPENCE, *Does the Helmholtz boundary element method suffer from the pollution effect?*, SIAM Rev., 65 (2023), pp. 806–828.
- [16] M. J. GANDER AND H. ZHANG, *Fourier analysis of finite difference schemes for the Helmholtz equation: Sharp estimates and relative errors*, arXiv preprint arXiv:2501.16696, (2025).
- [17] M. HAUCK AND D. PETERSEIM, *Multi-resolution localized orthogonal decomposition for Helmholtz problems*, Multiscale Model. Simul., 20 (2022), pp. 657–684.
- [18] R. HIPTMAIR, A. MOIOLA, AND I. PERUGIA, *Plane wave discontinuous galerkin methods for the 2D helmholtz equation: Analysis of the p -version*, SIAM J. Numer. Anal., 49 (2011), pp. 264–284.
- [19] R. HIPTMAIR, A. MOIOLA, AND I. PERUGIA, *Trefftz discontinuous Galerkin methods for acoustic scattering on locally refined meshes*, Appl. Numer. Math., 79 (2014), pp. 79–91.
- [20] R. HIPTMAIR, A. MOIOLA, AND I. PERUGIA, *A survey of Trefftz methods for the Helmholtz equation*, in Building Bridges: Connections and Challenges in Modern Approaches to Numerical Partial Differential Equations, G. R. Barrenechea, F. Brezzi, A. Cangiani, and E. H. Georgoulis, eds., vol. 114, 2016, pp. 237–279.
- [21] F. IHLBURG AND I. BABUŠKA, *Finite element solution of the Helmholtz equation with high wave number. Part I: The h-version of the FEM*, Comput. Math. Appl., 30 (1995), pp. 9–37.
- [22] F. IHLBURG AND I. BABUŠKA, *Finite element solution of the Helmholtz equation with high wave number. part II: The h-p version of the FEM*, SIAM J. Numer. Anal., 34 (1997), pp. 315–358.
- [23] D. LAFONTAINE, E. SPENCE, AND J. WUNSCH, *Wavenumber-explicit convergence of the hp-FEM for the full-space heterogeneous Helmholtz equation with smooth coefficients*, Comput. Math. Appl., 113 (2022), pp. 59–69.
- [24] J. MELENK AND S. SAUTER, *Convergence analysis for finite element discretizations of the Helmholtz equation with Dirichlet-to-Neumann boundary conditions*, Math. Comput., 79 (2010), pp. 1871–1914.
- [25] J. M. MELENK, A. PARSANIA, AND S. SAUTER, *General DG-methods for highly indefinite Helmholtz problems*, J. Sci. Comput., 57 (2013), pp. 536–581.
- [26] J. M. MELENK AND S. SAUTER, *Wavenumber explicit convergence analysis for Galerkin discretizations of the Helmholtz equation*, SIAM J. Numer. Anal., 49 (2011), pp. 1210–1243.
- [27] D. PETERSEIM, *Eliminating the pollution effect in Helmholtz problems by local subscale correction*, Math. Comput., 86 (2017), pp. 1005–1036.
- [28] B. H. QIWEI FENG AND M. MICHELLE, *Sixth-order compact finite difference method for 2D Helmholtz equations with singular sources and reduced pollution effect*, Commun. Comput. Phys., 34 (2023), pp. 672–712.
- [29] D. SCHARFETTER AND H. GUMMEL, *Large-signal analysis of a silicon read diode oscillator*, IEEE Trans. Electron. Devices, 16 (1969), pp. 64–77.
- [30] K. WANG AND Y. S. WONG, *Pollution-free finite difference schemes for non-homogeneous Helmholtz equation*, Int. J. Numer. Anal. Model., 11 (2014).
- [31] Y. S. WONG AND G. LI, *Exact finite difference schemes for solving Helmholtz equation at any wavenumber*, Int. J. Numer. Anal. Model., Series B, 2 (2011), pp. 91–108.
- [32] T. WU AND R. XU, *An optimal compact sixth-order finite difference scheme for the Helmholtz equation*, Comput. Math. Appl., 75 (2018), pp. 2520–2537.

INSTITUTE OF ANALYSIS AND SCIENTIFIC COMPUTING, TU WIEN, WIEDNER HAUPTSTRASSE 8–10,
1040 WIEN, AUSTRIA

Email address: juengel@tuwien.ac.at

SCHOOL OF MATHEMATICAL SCIENCES, SOOCHOW UNIVERSITY, SUZHOU, 215006, CHINA

Email address: lipch@suda.edu.cn

INSTITUTE OF ANALYSIS AND SCIENTIFIC COMPUTING, TU WIEN, WIEDNER HAUPTSTRASSE 8–10,
1040 WIEN, AUSTRIA

Email address: zhiwei.sun@tuwien.ac.at

DEPARTMENT OF MATHEMATICS, THE UNIVERSITY OF HONG KONG, HONG KONG, CHINA

Email address: zhangzw@hku.hk